Full Paper

www.molinf.com

molecular informatics

SPECIAL ISSUE

DOI: 10.1002/minf.201501034

Rational design, synthesis and evaluation of coumarin derivatives as protein-protein interaction inhibitors

Laura De Luca,*[a] Fatima E. Agharbaoui,*[a] Rosaria Gitto,[a] Maria Rosa Buemi,[a] Frauke Christ,[b] Zeger Debyser,[b] and Stefania Ferro[a]

Abstract: Herein we describe the design and synthesis of a new series of coumarin derivatives searching for novel HIV-1 integrase (IN) allosteric inhibitors. All new obtained compounds were tested in order to evaluate their ability to inhibit the interaction between the HIV-1 IN enzyme and the nuclear protein lens epithelium growth factor LEDGF/p75. A combined approach of docking and molecular dynamic simulations has been applied to clarify the activity of the new compounds. Specifically, the binding free energies by using the method of molecular mechanics-generalized Born surface area (MM-GBSA) was calculated, whereas hydrogen bond occupancies were monitored throughout simulations methods.

Keywords: HIV-1 · IN · LEDGF/p75 · Docking · Molecular Dynamics

1 Introduction

Since the discovery of HIV-1, the etiological agent of the acquired immune deficiency syndrome (AIDS), 26 antiretroviral compounds have been approved by the US Food and Drug Administration (FDA). Based on "Global AIDS Response Progress Reporting 2015"[1] there are nearly 15 million of people receiving the therapy.[2] The current most effective AIDS treatment, referred as combinatorial AntiRetroviral Therapy (cART), includes reverse transcriptase inhibitors (RTIs), protease inhibitors (PIs), fusion inhibitors (FIs), coreceptor inhibitors (CRIs) and integrase inhibitors (INIs), used in combination regimens.[3–6]

As consequence of these medical advances the AIDS-related mortality has dropped sharply reducing in incidence, and the syndrome has gradually become a controllable chronic disease.

However, it was recently demonstrated that low-level of viremia (LLV) of HIV-1 in the plasma is relatively common among patients on cART regimen.[7–10] This phenomenon is often associated with a greater risk of virologic failure as emergence of drug resistance and immune activation.

Moreover the need for lifelong treatment, the frequently associated toxic effects, anatomical barriers and also the existence of virus-reservoirs are some of the obstacles in the severely hurt patients compliance, a decisive factor in achieving a successful response to cART in HIV-1 infection.

Thus, the development of safer and potentially promising antiretroviral agents is eagerly needed, and considerable efforts have been made to identify new molecules capable of suppressing drug-resistant HIV-1 strains and/or targeting different stages in the virus life cycle.

It is now widely known that the stability of HIV-1 infection critically depends on the HIV-1 Integrase (IN) mediated integration of viral DNA into the host genome, an highly organized multistep process that relies on several cellular proteins for completion. So an alternative approach to block the HIV-1 integration step, instead of targeting directly the catalytic activity of IN, is to interfere with the interaction between the enzyme and the cellular cofactors, stopping integration in allosteric way.

Among several identified IN cofactors, lens epithelium-derived growth factor or transcriptional co-activator p75 (LEDGF/p75) is emerged as a target of great interest for the development of a novel generation of integration inhibitors.[11–14]

LEDGF/p75 binds to the interface of IN dimer and promotes IN tetramerization of enzyme resulting in the functional form of IN required for concerted integration.[15] So, after the initial identification and validation of the interaction between LEDGF/p75 and the enzyme[16–17] a crucial role for this cofactor in HIV-1 replication was evidenced through different mutagenesis, transdominant and knockout studies.[18–22] In the last decade some compounds have been discovered as promising LEDGF/p75 inhibitors. Figure 1 displays the most representative compounds from different chemical classes.[12,23–29]

[a] *L. De Luca, F. E. Agharbaoui, R. Gitto, M. R. Buemi, S. Ferro*
Dipartimento di Scienze Chimiche, Biologiche Farmaceutiche ed Ambientali, Università degli Studi di Messina
Viale Annunziata, I-98168, Messina, Italy
**e-mail: ldeluca@unime.it*
fagharbaoui@unime.it

[b] *F. Christ, Z. Debyser*
Molecular Virology and Gene Therapy KU Leuven and IRC KULAK
Kapucijnenvoer 33, B-3000 Leuven, Flanders, Belgium

Considering that Natural Products (NPs) have historically represented a remarkably source for new medicines as well as the origin of lead compounds,[30–31] we have recently reported the application of a virtual screening strategy to access novel drug-like natural compounds as potential protein-protein interaction inhibitors (PPIIs). As results, new hit structures from natural sources proved to be active as PPIIs of the IN-LEDGF/p75 complex. Among them, we selected the 8-methyl-2-oxo-4-phenyl-2H-chromen-7-yl)oxy](phenyl)-acetic acid (**CR**) (Figure 1) structurally characterized by coumarin nucleus. It is well-known that coumarins are a versatile class of heterocycles displaying a wide range of therapeutic activities. Particularly, coumarin derivatives have been shown to be pharmacologically useful as anti-coagulants, anti-oxidants, antitumorals, free radical scavengers and also anti-HIV agents.[32–38]

It is interesting to note that the 4-phenylcoumarin core of hit compound **CR** resembles the heterocyclic systems of inhibitors **CX5016**, **BI1001** and **CX14442** depicted in Figure 1. Moreover, **CR** and other LEDGF/p75 inhibitors share the carboxylate function, for which has been demonstrated a pivotal role in the inhibition of IN-LEDGF/p75 interaction.[14,23]

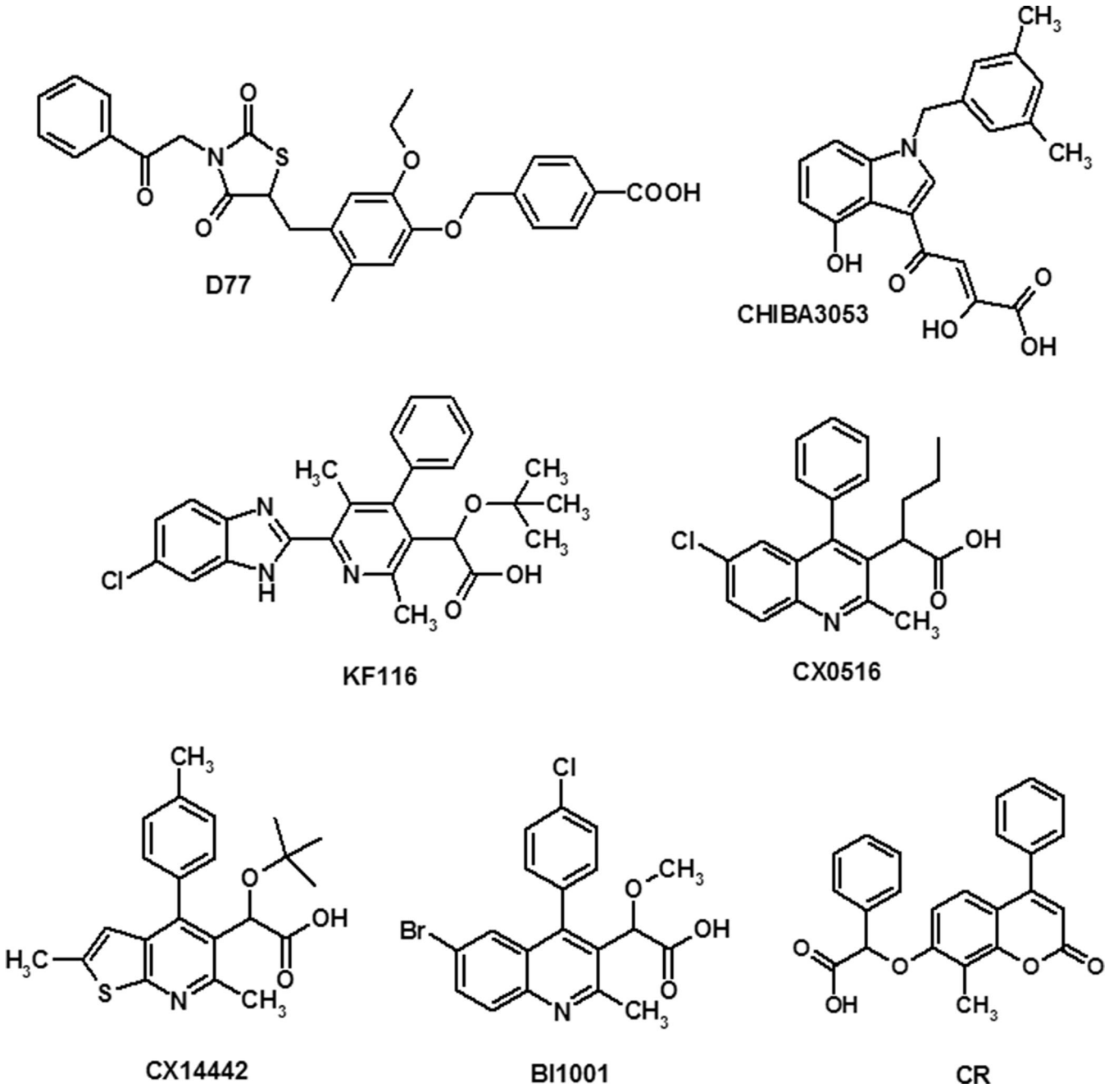

Figure 1. Chemical structures of well-known LEDGF/p75 inhibitors.

In the current work several structural modifications, computational studies and biological screening of new 4-phenylcoumarin derivatives are presented with the aim of achieving further information about the mechanism of inhibition of IN-LEDGF/p75 interaction.

2 Experimental Section

2.1 Chemistry

All starting materials and reagents commercially available (Sigma-Aldrich Milan Italy and Alfa Aesar Karlsruhe Germany) were used without further purification. Microwave-assisted reactions were carried out in a CEM Focused Microwave Synthesis System Model Discover working at the power necessary for refluxing under atmospheric conditions. Melting points were determined on a BUCHI Melting Point B-545 apparatus and are uncorrected.

Elemental analysis (C, H, N) were carried out on a Carlo Erba Model 1106 Elemental Analyzer and the results are within $\pm 0.4\%$ of the theoretical values. Merck silica gel 60 F_{254} plates were used for analytical TLC; column chromatography was performed on Merck silica gel 60 (230–400 mesh). Flash Chromatography (FC) was carried out on a Biotage SP_1 EXP. ^{1}H-NMR spectra were recorded in $CDCl_3$ with TMS as internal standard or [D_6]DMSO on a Varian Gemini-300 spectrometer. Chemical shifts were expressed in δ (ppm) and coupling constants (*J*) in Hertz (Hz). All exchangeable protons were confirmed by addition of D_2O. Mass spectrometry analysis were realized on Bruker MicrOTOF (ESI) equipped with an Agilent 1200 LC.

General procedures for the synthesis of 7-hydroxy-2*H*-chromen-2-ones. (4 and 7–14)

Compounds **4** and **7–14** were prepared by reaction of resorcinol (**1**), 2-chlororesorcinol (**2**) or 2-methylresorcinol (**3**) (1 mmol) with malic acid or with the appropriate ethyl benzoylacetate (1.2 mmol), in aqueous 70% sulfuric acid (2 mL). The resulting solution was stirred at room temperature for 3 hours and then was poured into ice. The obtained precipitate was filtered, washed with water, dried and crystallized with ethanol.

7-Hydroxy-8-methyl-2*H*-chromen-2-one (4)

Mp: 195–197°, yield 49%. ^{1}H NMR (DMSO-d_6): 2.15 (s, 3H, CH_3), 6.22 (d, 1H, *J* = 8.8, CH), 6.82 (d, 1H, *J* = 8.2, CH), 7.90 (d, 1H, *J* = 9.4, ArH), 8.00 (d, 1H, *J* = 9.3, ArH), 10.48 (bs, 1H, OH). Anal. ($C_{10}H_8O_3$).

7-Hydroxy-4-phenyl-2*H*-chromen-2-one (7)

Mp: 195–197°, yield 53%. ^{1}H NMR (DMSO-d_6): 6.14 (s, 1H, CH), 6.76–6.80 (m, 2H, ArH), 7.27 (d, *J* = 8.2, 1H, ArH), 7.49–7.56 (m, 5H, ArH), 10.65 (bs, 1H, OH). Anal. ($C_{15}H_{10}O_3$).

8-Chloro-7-hydroxy-4-phenyl-2H-chromen-2-one (8)

Mp: 214–215°, yield 41%. ^{1}H NMR ($CDCl_3$): 5.89 (s, 1H, CH), 6.66 (d, *J* = 8.8, 1H, ArH), 6.95 (d, *J* = 8.8, 1H, ArH), 7.15–7.25 (m, 5H, ArH). Anal. ($C_{15}H_9ClO_3$).

4-(2-Chlorophenyl)-7-hydroxy-8-methyl-2*H*-chromen-2-one (9)

Mp: 240–242°, yield 70%. ^{1}H NMR (DMSO-d_6): 2.18 (s, 3H, CH_3), 6.15 (s, 1H, CH), 6.65 (d, *J* = 8.8, 1H, ArH), 6.77 (d, *J* = 8.8, 1H, ArH), 7.41–7.65 (m, 4H, ArH), 10.56 (bs, 1H, OH). Anal. ($C_{16}H_{11}ClO_3$).

4-(3-Chlorophenyl)-7-hydroxy-8-methyl-2*H*-chromen-2-one (10)

Mp: 315–317°, yield 79%. ^{1}H NMR (DMSO-d_6): 2.18 (s, 3H, CH_3), 6.18 (s, 1H, CH), 6.83 (d, *J* = 8.5, 1H, ArH), 7.04 (d, *J* = 9.0, 1H, ArH), 7.44 (d, *J* = 8.5, 1H, ArH), 7.53–7.59 (m, 3H, ArH), 10.59 (bs, 1H, OH). Anal. ($C_{16}H_{11}ClO_3$).

4-(4-Chlorophenyl)-7-hydroxy-8-methyl-2*H*-chromen-2-one (11)

Mp: 253–255°, yield 87%. ^{1}H NMR (DMSO-d_6): 2.19 (s, 3H, CH_3), 6.15 (s, 1H, CH), 6.83 (d, *J* = 9.0, 1H, ArH), 7.08 (d, *J* = 9.0, 1H, ArH), 7.50 (d, *J* = 9.0, 2H, ArH), 7.61 (d, *J* = 8.5, 2H, ArH), 10.55 (bs, 1H, OH). Anal. ($C_{16}H_{11}ClO_3$).

7-Hydroxy-8-methyl-4-(2-methylphenyl)-2*H*-chromen-2-one (12)

Mp: 108–110°, yield 26%. ^{1}H NMR (DMSO-d_6): 2.07 (s, 3H, CH_3), 2.18 (s, 3H, CH_3), 6.06 (s, 1H, CH), 6.64 (d, *J* = 8.2, 1H, ArH), 6.76 (d, *J* = 8.8, 1H, ArH), 7.19 (d, *J* = 7.6, 1H, ArH), 7.31–7.40 (m, 3H, ArH), 10.53 (bs, 1H, OH). Anal. ($C_{17}H_{14}O_3$).

7-Hydroxy-8-methyl-4-(3-methylphenyl)-2*H*-chromen-2-one (13)

Mp: 181–183°, yield 88%. ^{1}H NMR (DMSO-d_6): 2.19 (s, 3H, CH_3), 2.38 (s, 3H, CH_3), 6.10 (s, 1H, CH), 6.82 (d, *J* = 8.8, 1H, ArH), 7.12 (d, *J* = 8.8, 1H, ArH), 7.27–7.43 (m, 4H, ArH), 10.56 (bs, 1H, OH). Anal. ($C_{17}H_{14}O_3$).

7-Hydroxy-8-methyl-4-(4-methylphenyl)-2*H*-chromen-2-one (14)

Mp: 259–261°, yield 63%. ^{1}H NMR (DMSO-d_6): 2.19 (s, 3H, CH_3), 2.38 (s, 3H, CH_3), 6.09 (s, 1H, CH), 6.82 (d, *J* = 8.5, 1H, ArH), 7.13 (d, *J* = 8.5, 1H, ArH), 7.35–7.37 (m, 4H, ArH), 10.53 (bs, 1H, OH). Anal. ($C_{17}H_{14}O_3$).

General procedures for the synthesis of ethyl [(2-oxo-4-phenyl-2*H*-chromen-7-yl)oxy]acetates (5 and 15–22)

To a well-stirred solution of 7-hydroxy-2H-chromen-2-one (**4**, **7–14**) (1 mmol) and potassium carbonate (5 mmol), in absolute acetone (3 mL), the appropriate ethyl bromophenyl acetate (1.2 mmol) was added dropwise. The reaction mixture was stirred and refluxed for 5 h at 110°. After that time the mixture was cooled to room temperature and filtered to remove the inorganic material. The solution was evaporated in vacuo to give the crude product. The residue was purified by crystallization with ethanol.

Ethyl [(8-methyl-2-oxo-2H-chromen-7-yl)oxy](phenyl)-acetate (5)

Mp: 125–126°, yield 73%. ^{1}H NMR ($CDCl_3$): 1.19 (t, *J* = 7.1, 3H, CH_3), 2.45 (s, 3H, CH_3),4.18 (q, *J* = 7.1, 2H, CH_2), 5.71 (s, 1H, CH), 6.26 (d, *J* = 9.3, 1H, CH), 6.72 (d, *J* = 8.2, 1H, CH), 7.21–7.62 (m, 7H, ArH). Anal. ($C_{20}H_{18}O_5$).

Ethyl [(2-oxo-4-phenyl-2*H*-chromen-7-yl)oxy](phenyl)-acetate (15)

Mp: 102–104°, yield 92%. ^{1}H NMR (DMSO-d_6): 1.11 (t, *J* = 7.1, 3H, CH_3), 4.15 (q, *J* = 7.1, 2H, CH_2), 6.23 (s, 1H, CH), 6.25 (s, 1H, CH), 7.00 (d, *J* = 8.8, 1H, ArH), 7.10 (s, 1H, ArH), 7.36

(d, $J=8.8$, 1H, ArH), 7.41–7.58 (m, 10H, ArH). Anal. ($C_{25}H_{20}O_5$).

Ethyl [(8-chloro-2-oxo-4-phenyl-2H-chromen-7-yl)oxy](phenyl)acetate (16)

Mp: 175–176°, yield 54%. ^{1}H NMR (DMSO-d_6): 1.11 (t, $J=7.1$, 3H, CH_3), 4.14 (q, $J=7.1$, 2H, CH_2), 6.24 (s, 1H, CH), 6.26 (s, 1H, CH), 6.92 (d, $J=8.9$, 1H, ArH), 7.35 (d, $J=8.9$, 1H, ArH), 7.40–7.60 (m, 10H, ArH). Anal. ($C_{25}H_{19}ClO_5$).

Ethyl {[8-methyl-4-(2-chlorophenyl)-2-oxo-2*H*-chromen-7-yl]oxy}(phenyl)acetate (17)

Mp: 188–190 °C, yield 96%. ^{1}H NMR (DMSO-d_6): 1.23 (t, $J=7.4$, 3H, CH_3), 2.33 (s, 3H, CH_3), 4.10 (q, $J=7.4$, 2H, CH_2), 6.18 (s, 1H, CH), 6.29 (s, 1H, CH), 6.76 (t, $J=8.8$, 1H, ArH), 6.93 (d, $J=8.8$, 1H, ArH), 7.39–7.65 (m, 9H, ArH). Anal. ($C_{26}H_{21}O_5$).

Ethyl {[8-methyl-4-(3-chlorophenyl)-2-oxo-2*H*-chromen-7-yl]oxy}(phenyl)acetate (18)

Mp: 187–189°, yield 77%. ^{1}H NMR (DMSO-d_6): 1.21 (t, $J=7.3$, 3H, CH_3), 2.34 (s, 3H, CH_3), 4.10 (q, $J=7.3$, 2H, CH_2), 6.21 (s, H, CH), 6.31 (s, 1H, CH), 6.99 (d, $J=9.4$, 1H, ArH), 7.15 (d, $J=8.8$, 1H, ArH), 7.41–7.47 (m, 4H, ArH), 7.57–7.60 (m, 5H, ArH). Anal. ($C_{26}H_{21}O_5$).

Ethyl {[8-methyl-4-(4-chlorophenyl)-2-oxo-2*H*-chromen-7-yl]oxy}(phenyl)acetate (19)

Mp: 194–196°, yield 98%. ^{1}H NMR (DMSO–d_6): 1.11 (t, $J=7.5$, 3H, CH_3), 2.34 (s, 3H, CH_3), 4.02 (q, $J=7.5$, 2H, CH_2), 6.22 (s, 1H, CH), 6.28 (s, 1H, CH), 6.99 (d, $J=9.4$, 1H, ArH), 7.19 (d, $J=8.8$, 1H, ArH), 7.41–7.47 (m, 3H, ArH), 7.44 (d, $J=8.8$, 2H, ArH), 7.57–7.63 (m, 4H, ArH). Anal. ($C_{26}H_{21}O_5$).

Ethyl {[8-methyl-4-(2-methylphenyl)-2-oxo-2*H*-chromen-7-yl]oxy}(phenyl)acetate (20)

Mp: 167–169°, yield 55%. ^{1}H NMR (DMSO-d_6): 1.07 (t, $J=7.0$, 3H, CH_3), 2.09 (s, 3H, CH_3), 2.34 (s, 3H, CH_3), 4.10 (q, 2H, $J=7.0$, CH_2), 6.13 (s, 1H, CH), 6.20 (s, 1H, CH), 6.75 (d, $J=8.8$, 1H, ArH), 6.93 (d, $J=8.8$, 1H, ArH), 7.17–7.45 (m, 7H, ArH), 7.55–7.59 (m, 2H, ArH). Anal. ($C_{27}H_{24}O_5$).

Ethyl {[8-methyl-4-(3-methylphenyl)-2-oxo-2*H*-chromen-7-yl]oxy}(phenyl)acetate (21)

Mp: 181° dec., yield 98%. ^{1}H NMR (DMSO-d_6): 1.09 (t, $J=7.0$, 3H, CH_3), 2.34 (s, 3H, CH_3), 2.38 (s, 3H, CH_3), 4.10 (q, $J=7.0$, 2H, CH_2), 6.17 (s, 1H, CH), 6.22 (s, 1H, CH), 6.99 (d, $J=9.3$, 1H, ArH), 7.21–7.46 (m, 8H, ArH), 7.58 (d, $J=9.4$, 2H, ArH). Anal. ($C_{27}H_{24}O_5$).

Ethyl {[8-methyl-4-(4-methylphenyl)-2-oxo-2*H*-chromen-7-yl]oxy}(phenyl)acetate (22)

Mp: 148–150°, yield 56%. ^{1}H NMR (DMSO-d_6): 1.09 (t, $J=7.0$, 3H, CH_3), 2.34 (s, 3H, CH_3), 2.39 (s, 3H, CH_3), 4.10 (q, $J=7.0$, 2H, CH_2), 6.17 (s, 1H, CH), 6.21 (s, 1H, CH), 6.99 (d, $J=9.4$, 1H, ArH), 7.24 (d, $J=8.8$, 1H, ArH), 7.34–7.60 (m, 9H, ArH). Anal. ($C_{27}H_{24}O_5$).

General procedures for the synthesis of [(2-oxo-4-phenyl-2*H*-chromen-7-yl)oxy]acetic acids. (6 and 23–30)

Derivatives **5**, **15**–**22** (1 mmol) were solubilized in ethanol (5 mL), treated with a water solution of NaOH (5N, 2 mL) and stirred at room temperature for 1.5 h. Then the reaction mixture was acidified with conc. HCl to afford a solid that was collected and crystallized with ethanol to give the carboxylic acid derivatives **6** and **15**–**22**.

[(8-Methyl-2-oxo-2*H*-chromen-7-yl)oxy](phenyl)acetic acid (6)

Mp: Dec, yield 89%. ^{1}H NMR ($CDCl_3$): 2.33 (s, 3H, CH_3), 5.63 (s, 1H, CH), 5.68 (s, 1H, CH), 6.46 (s, 1H, CH), 6.96–7.60 (m, 7H, ArH). Anal. Calcd for $C_{18}H_{14}O_5$. ESI(−), CH_3OH, HR-MS : ion [M−H]−, m/z 310, $C_{18}H_{14}O_5$, m/z theory 310,09, m/z found 309,08.

[(2-Oxo-4-phenyl-2*H*-chromen-7-yl)oxy](phenyl)acetic acid (23)

Mp: 240–242°, yield 62%. ^{1}H NMR (DMSO-d_6): 6.06 (s, 1H, CH), 6.24 (s, 1H, CH), 7.00 (dd, $J=8.8$, $J=9.3$, 1H, ArH), 7.08 (d, 1H, $J=2.3$, ArH), 7.35 (d, $J=8.8$, 1H, ArH), 7.39–7.58 (m, 10H, ArH). Anal. Calcd for $C_{23}H_{16}O_5$. ESI(−), CH_3OH, HR-MS : ion [M−H]−, m/z 372, $C_{23}H_{16}O_5$, m/z theory 372,10, m/z found 371,09.

[(8-Chloro-2-oxo-4-phenyl-2H-chromen-7-yl)oxy](phenyl)acetic acid (24)

Mp: 220–222°, yield 98%. ^{1}H NMR (DMSO-d_6): 6.16 (s, 1H, CH), 6.33 (s, 1H, CH), 7.13 (d, $J=9.4$, 1H, ArH), 7.34–7.61 (m, 10H, ArH), 7.71 (d, $J=8.7$, 1H, ArH). Anal. Calcd for $C_{23}H_{15}ClO_5$. ESI(−), CH_3OH, HR-MS: ion [M−H]−, m/z 406, $C_{23}H_{15}ClO_5$, m/z theory 406,06, m/z found 405,05.

{[4-(2-Chlorophenyl)-8-methyl-2-oxo-2*H*-chromen-7-yl]oxy}(phenyl) acetic acid (25)

Mp: 262–264°, yield 99%. ^{1}H NMR (DMSO-d_6): 2.34 (s, 3H, CH_3), 6.03 (s, 1H, CH), 6.29 (s, 1H, CH), 6.79 (d, $J=9.0$ 1H, ArH), 6.94 (d, $J=8.8$, 1H, ArH), 7.40–7.66 (m, 9H, ArH). Anal. Calcd for $C_{24}H_{17}ClO_5$. ESI(−), CH_3OH, HR-MS: ion [M−H]−, m/z 420, $C_{24}H_{17}ClO_5$, m/z theory 420,08, m/z found 419,07.

{[4-(3-Chlorophenyl)-8-methyl-2-oxo-2*H*-chromen-7-yl]oxy}(phenyl) acetic acid (26)

Mp: 295° dec., yield 99%. ^{1}H NMR (DMSO-d_6): 2.34 (s, 3H, CH_3), 6.05 (s, 1H, CH), 6.30 (s, 1H, CH), 6.99 (d, $J=9.4$ 1H, ArH), 7.16 (d, $J=8.8$, 1H, ArH), 7.40–7.46 (m, 4H, ArH), 7.57–7.61 (m, 5H, ArH). Anal. Calcd for $C_{24}H_{17}ClO_5$. ESI(−), CH_3OH, HR-MS : ion [M−H]−, m/z 420, $C_{24}H_{17}ClO_5$, m/z theory 420,08, m/z found 419,07.

{[4-(4-Chlorophenyl)-8-methyl-2-oxo-2*H*-chromen-7-yl]oxy}(phenyl) acetic acid (27)

Mp: 246–248°, yield 99%. ^{1}H NMR (DMSO-d_6): 2.33 (s, 3H, CH_3), 6.05 (s, 1H, CH), 6.26 (s, 1H, CH), 6.97 (d, $J=9.1$, 1H, ArH), 7.18 (d, $J=8.5$, 1H, ArH), 7.37–7.53 (m, 5H, ArH), 7.57–7.61 (m, 4H, ArH). Anal. Calcd for $C_{24}H_{17}ClO_5$. ESI(−), CH_3OH, HR-MS : ion [M−H]−, m/z 420, $C_{24}H_{17}ClO_5$, m/z theory 420,08, m/z found 419,07.

{[8-Methyl-4-(2-methylphenyl)-2-oxo-2*H*-chromen-7-yl]oxy}(phenyl) acetic acid (28)

Mp: 114–117°, yield 61%. ^{1}H NMR (DMSO-d_6): 2.07 (s, 3H, CH_3), 2.34 (s, 3H, CH_3), 6.00 (s, 1H, CH), 6.19 (s, 1H, CH), 6.76 (d, $J=8.8$ 1H, ArH), 6.92 (d, $J=8.2$, 1H, ArH), 7.20–7.45 (m, 7H, ArH), 7.44–7.58 (m, 2H, ArH). Anal. Calcd for $C_{25}H_{20}O_5$. ESI(−), CH_3OH, HR-MS : ion [M−H]−, m/z 400, $C_{25}H_{20}O_5$, m/z theory 400,13, m/z found 399,12.

{[8-Methyl-4-(3-methylphenyl)-2-oxo-2*H*-chromen-7-yl]oxy}(phenyl) acetic acid (29)

Mp: 107–109°, yield 32%. ^{1}H NMR (DMSO-d_6): 2.34 (s, 3H, CH_3), 2.38 (s, 3H, CH_3), 5.95 (s, 1H, CH), 6.21 (s, 1H, CH), 6.97 (d, J=8.8, 1H, ArH), 7.20–7.43 (m, 8H, ArH), 7.59 (d, J=8.2, 2H, ArH). Anal. Calcd for $C_{25}H_{20}O_5$. ESI(−), CH_3OH, HR-MS : ion [M−H]−, m/z 400, $C_{25}H_{20}O_5$, m/z theory 400,13, m/z found 399,12.

{[8-Methyl-4-(4-methylphenyl)-2-oxo-2*H*-chromen-7-yl]oxy}(phenyl) acetic acid (30)

Mp: 263° dec., yield 97%. ^{1}H NMR (DMSO-d_6): 2.33 (s, 3H, CH_3), 2.38 (s, 3H, CH_3), 6.03 (s, 1H, CH), 6.19 (s, 1H, CH), 6.99 (d, J=9.3, 1H, ArH), 7.25 (d, J=8.8, 1H, ArH), 7.36–7.43 (m, 7H, ArH), 7.60 (m, 2H, ArH). Anal. Calcd for $C_{25}H_{20}O_5$. ESI(−), CH_3OH, HR-MS : ion [M−H]−, m/z 400, $C_{25}H_{20}O_5$, m/z theory 400,13, m/z found 399,12.

Synthesis of 7-hydroxy-8-methyl-4-phenyl-2*H*-chromen-2-one (31)

Ethyl benzoylacetate (1.2 mmol) was added to a solution of 2-methylresorcinol (1 mmol) in aqueous 70% sulfuric acid solution (2 mL). The resulting mixture was stirred at room temperature for 3 hours and then was poured into ice. The obtained precipitate was filtered, washed with water, dried and crystallized with ethanol.

Mp: 223–225°, yield 93 %. ^{1}H NMR (DMSO-d_6): 2.19 (s, 3H, CH_3), 6.12 (s, 1H, CH), 6.82 (d, J=8.8, 1H, ArH), 7.11 (d, J=8.5, 1H, ArH), 7.46–7.55 (m, 5H, ArH), 10.54 (bs, 1H, OH). Anal. ($C_{16}H_{12}O_3$).

General procedures for the synthesis of ethyl [(8-methyl-2-oxo-4-phenyl-2*H*-chromen-7-yl)oxy]acetate (32) and ethyl 2-[(8-methyl-2-oxo-4-phenyl-2*H*-chromen-7-yl)oxy]propanoates (33–34)

To a solution of 7-hydroxy-8-methyl-4-phenyl-2*H*-chromen-2-one **(31)** (1 mmol) in absolute acetone (3 mL), potassium carbonate (5 mmol) and the appropriate ethyl bromophenyl acetate (1.2 mmol) were added. The mixture was heated to reflux for 5 h, until TLC indicated the disappearance of the starting material. Then, it was cooled to 0 °C and filtered to remove the inorganic material. The solution was evaporated in vacuo to give the crude product. The residue was purified by crystallization with ethanol.

Ethyl [(8-methyl-2-oxo-4-phenyl-2*H*-chromen-7-yl)oxy]-acetate (32)

Mp: 143–145°, yield 54%. ^{1}H NMR (DMSO-d_6): 1.19 (t, J=7.2, 3H, CH_3), 2.28 (s, 3H, CH_3), 4.15 (q, J=7.2, 2H, CH_2), 4.94 (s, 2H, CH_2), 6.24 (s, 1H, CH), 6.93 (d, J=9.1, 1H, ArH), 7.21 (d, J=9.0, 1H, ArH), 7.49–7.57 (m, 5H, ArH). Anal. ($C_{20}H_{18}O_5$).

Ethyl 2-[(8-methyl-2-oxo-4-phenyl-2*H*-chromen-7-yl)-oxy]propanoate (33)

Mp: 136–138°, yield 51%. ^{1}H NMR (DMSO-d_6): 1.15 (t, J=6.9, 3H, CH_3), 1.55 (d, J=6.9, 3H, CH_3), 2.27 (s, 3H, CH_3), 4.11 (q, J=6.9, 2H, CH_2), 5.10 (q, J=6.9, 1H, CH), 6.24 (s, 1H, CH), 6.87 (d, J=9.0, 1H, ArH), 7.20 (d, J=9.1, 1H, ArH), 7.48–7.56 (m, 5H, ArH). Anal. ($C_{21}H_{20}O_5$).

Ethyl 2-methyl-2-[(8-methyl-2-oxo-4-phenyl-2*H*-chromen-7-yl)oxy]propanoate (34)

Mp: 121–123°, yield 81%. ^{1}H NMR (DMSO-d_6): 1.14 (t, J=7.1, 3H, CH_3), 1.58 (s, 6H, $2CH_3$), 2.26 (s, 3H, CH_3), 4.15 (q, J=7.1, 2H, CH_2), 6.25 (s, 1H, CH), 6.64 (d, J=9.4, 1H, ArH), 7.21 (d, J=8.8, 1H, ArH), 7.49–7.57 (m, 5H, ArH). Anal. ($C_{22}H_{22}O_5$).

General procedures for the synthesis of [(8-methyl-2-oxo-4-phenyl-2H-chromen-7-yl)oxy]acetic acid (35) and 2-[(8-methyl-2-oxo-4-phenyl-2*H*-chromen-7-yl)oxy]propanoic acids (35–37)

The intermediates **(33–34)** obtained in the previous step were deprotected according to procedure previously described for compounds **6** and **23–30.**

[(8-Methyl-2-oxo-4-phenyl-2H-chromen-7-yl)oxy]acetic acid (35)

Mp: 233–235°, yield 99%. ^{1}H NMR (DMSO-d_6): 2.27 (s, 3H, CH_3), 4.83 (s, 2H, CH_2), 6.23 (s, 1H, CH), 6.93 (d, J=9.0 1H, ArH), 7.21 (d, J=9.1, 1H, ArH), 7.45–7.56 (m, 5H, ArH). Anal. Calcd for $C_{18}H_{14}O_5$. ESI(−), CH_3OH, HR-MS : ion [M−H]−, m/z 310, $C_{18}H_{14}O_5$, m/z theory 310,09, m/z found 309,08.

2-[(8-Methyl-2-oxo-4-phenyl-2*H*-chromen-7-yl)oxy]propanoic acid (36)

Mp: 236–238°, yield 98%. ^{1}H NMR (DMSO-d_6): 1.54 (d, J=6.9, 3H, CH_3), 2.26 (s, 3H, CH_3), 5.01 (q, J=6.9, 1H, CH), 6.22 (s, 1H, CH), 6.86 (d, J=9.0, 1H, ArH), 7.20 (d, J=9.0, 1H, ArH), 7.46–7.55 (m, 5H, ArH). Anal. Calcd for $C_{19}H_{16}O_5$. ESI(−), CH_3OH, HR-MS : ion [M−H]−, m/z 324, $C_{19}H_{16}O_5$, m/z theory 324,10, m/z found 323,09.

2-Methyl-2-[(8-methyl-2-oxo-4-phenyl-2*H*-chromen-7-yl)oxy]propanoic acid (37)

Mp: 122–124°, yield 71%. ^{1}H NMR (DMSO-d_6): 1.57 (s, 6H, $2CH_3$), 2.25 (s, 3H, CH_3), 6.23 (s, 1H, CH), 6.71 (d, J=8.8, 1H, ArH), 7.20 (d, J=8.8, 1H, ArH), 7.50–7.56 (m, 5H, ArH). Anal. Calcd for $C_{20}H_{18}O_5$. ESI(−), CH_3OH, HR-MS : ion [M−H]−, m/z 338, $C_{20}H_{18}O_5$, m/z theory 324,10, m/z found 337,10.

2.2 Biological Assays

2.2.1 LEDGF/p75-HIV-1 Integrase Interaction Screening

The AlphaScreen assay was performed as previously described.[46] Reactions were performed in 25 µl final volume in 384-well Optiwell™ microtiter plates (Perkin–Elmer). The reaction buffer contained 25 mM Tris–HCl (pH 7.4), 150 mM NaCl, 1 mM $MgCl_2$, 0.01% (v/v) Tween-20 and 0.1% (w/v) bovine serum albumin. His6-tagged integrase (300 nM final concentration) was incubated with the compounds at 4° for 30 min. The compounds were added in varying concentrations from 1 up to 100 nM. Afterwards 100 nM of recombinant flag-LEDGF/p75 was added and incubation was extended by another hour at 4°. Subsequently, 5 µl of Ni-chelate-coated acceptor beads and 5 µl of anti-flag donor beads were added to a final concentration of 20 µg/ml of both beads. Proteins and beads were incubated at 30° for 1 h in order to allow association to occur. Exposure of the reaction to direct light was prevented as much as possible and the emission of light from the acceptor beads was

measured in the EnVision plate reader (Perkin–Elmer, Benelux) and analyzed using the EnVision manager software.

2.2.2 In vitro Anti-HIV and Drug Susceptibility Assays

The inhibitory effect of antiviral drugs on the HIV-induced cytopathic effect (CPE) in human lymphocyte MT-4 cell culture was determined by the MT-4/MTT-assay.[53] This assay is based on the reduction of the yellow coloured 3-(4,5-dimethylthiazol-2-yl)-2,5-diphenyltetrazolium bromide (MTT) by mitochondrial dehydrogenase of metabolically active cells to a blue formazan derivative, which can be measured spectrophotometrically. The 50% cell culture infective dose ($CCID_{50}$) of the HIV(III_B) strain was determined by titration of the virus stock using MT-4 cells. For the drug-susceptibility assays, MT-4 cells were infected with 100–300 $CCID_{50}$ of the virus stock in the presence of five-fold serial dilutions of the antiviral drugs. The concentration of the various compounds that achieved 50% protection against the CPE of the different HIV strains, which is defined as the EC_{50}, was determined. In parallel the 50% cytotoxic concentration (CC_{50}) was determined.

2.3 Computational Studies

2.3.1 Docking Simulations

- Ligand preparation

3D structure of each ligand was constructed using Discovery Studio2.5.5 and minimized using CHARMmforcefield followed by Smart Minimizer algorithm performing 1000 steps of Steepest Descent with a root mean square (RMS) gradient tolerance of 3, followed by Conjugate Gradient minimization, until the RMS gradient for potential energy was less than 0.05 kcal/mol/Å.

- Protein preparation

The protein was prepared using Discovery Studio 2.5.5.[54]

For our docking simulations the crystal structure of the dimeric CCD of HIV-1 IN complexed with the IBD of LEDGF/p75 was retrieved from RCSB Protein Data Bank (PDB : 2B4J).[47] First, the LEDGF/p75 structure and the water molecules solved by X-ray crystallography were removed, then the missing hydrogens were added to the pattern.

- Validation of docking protocol

The validation of the docking protocol was performed by docking the native co-crystallized ligands of the two crystal structures with the PDB codes 3LPT and 3LPU, into LEDGF/p75 binding site. The comparison of docking results with the co-crystallized form showed success rates with the docked ligand strictly superimposed with the crystallized conformation with RMSD = 1.01 Å indicating that the used scoring function is successful. These values were small enough and supported the hypothesis that experimental binding modes could be reproduced with accuracy using this protocol. The standard default settings were used in all calculations.

- Docking studies

Docking studies were performed using the genetic optimization for ligand docking (GOLD) software package version 4.1.1 from the Cambridge Crystallographic Data Centre (CCDC)[50] as described in our previous paper.[42]

For the prediction of ligand binding positions GoldScore fitness function was used. For each ligand 100 independent runs and a maximum of 15000 genetic operations were performed using the default operator weights and a population size of 100 chromosomes.

Default cutoff values of 2.5 Å for hydrogen bonds and 4.0 Å for van der Waals interactions were employed. Automatic bond settings were used, allowing the torsion angles of all acyclic, rotatable bonds in the ligand to vary except for amide bonds. Results differing by less than 0.75 Å in ligand-all-atom RMSD were clustered together.

Results differing by less than 1.00 Å in ligand-all atom RMSD were clustered together. A 20.0 Å radius active site was drawn on the original position of the LEDGF/p75 IBD dipeptide Ile365-Asp366 and automated cavity detection was used. Two hydrogen bond constraints were used to specify that two protein atoms should be hydrogen-bonded to the ligand, namely NH backbone of Glu170 and His171 with a constraint weight of 5.

Binding energy of the minimized complex was calculated using the MM-GBSA method[51] implemented in the AMBER program.

2.3.2 Molecular Dynamics Simulations

- Model Preparation

The starting model for simulations of IN-LEDGF/p75 was prepared as described in our previous paper.[42] In brief, from the X-ray structure 2B4J of IN CCD (chains A and B) in complex with the $LEDGF_{IBD}$ (chains C and D)[47] was used. First, chain D and water molecules were removed from the structure. Then, the missing residues of the IN_{CCD} were added by superimposing chain C of the HIV-1 IN 1BL3[55] structure and energy-minimized using Maestro[56] with a RMSD of 0.30 Å. From the resulting complex, the chain C of $LEDGF_{IBD}$ was castoff in order to simulate IN-PPIIs complexes.

- Molecular Dynamics

MD simulations were carried out using the sander module of AMBER 11[52] and parm 99.dat and frcmod.ff03

parameter files.[57–58] These parameters were assigned to the designed ligands, while partial charges were calculated using the AM1-BCC method as implemented in the Antechamber suite of AMBER 11.

The geometry of the system was minimized in order to remove any bad contact using the steepest descent algorithm for the first 250 steps before switching to the conjugate gradient algorithm for the remaining 250 steps.

Solvent effects were taken into account by using the generalized Born implicit solvent model. The minimized structure was the input for MD runs using constant-temperature Langevin dynamics at 300 K for 100 ps with a time step of 1 fs and a distance cutoff of 12.0 Å for the nonbonded interactions.

- Analysis of MD Trajectories and Free Energy

Snapshots of the complexes during the simulations and the average structures were obtained with the Ptraj module of the AMBER 11 suite.[52]

The hydrogen bonds were detected when the acceptor-donor atom distance was lower than 3.5 Å and the acceptor-H-donor angle was more than 120°. The MM-GBSA method[51] implemented in the AMBER program was used to evaluate the ligand-protein interaction free energies of the minimized complex and the 100 snapshots extracted at 1 ps intervals.

For MM-GBSA analysis, snapshots at 40 ps intervals were extracted from the last 4 ns of the MD trajectory, and the binding free energies were averaged over the ensemble of conformers produced (100 snapshots for each trajectory).

3 Results and Discussion

3.1 Rational Design

As a continuation of our previous studies on anti-HIV agents and in particular on HIV-IN enzyme inhibitors,[11–12,27,39–45] herein we report the results of a research on PPIIs.

It is well known that the identification of small molecules able to interfere with IN-LEDGF/p75 interaction could provide an enormous impetus in the field of antiretroviral research.

Thus, in order to obtain useful insights for the development of new small molecules that specifically disrupt this PPI, we have previously investigated the most important contacts between some PPI inhibitors and the IN-LEDGF/p75 complex.[27]

By means of a combination of docking and ultrashort MD, we have generated a weighted ensemble of protein-ligand configurations and estimated the binding affinity averaged over snapshots taken from the MD trajectories, together with the presence of fundamental hydrogen bonds.[42]

All obtained information has been used in a virtual screening strategy that led to a selection of nine *in silico* hits that were tested in AlphaScreen assay[46] to evaluate their ability to prevent IN-LEDGF/p75 interaction. Eight of them have exhibited inhibitory effects at 100 μM ranging from 30% to 88% and for six of them the IC_{50} value was determined.[27]

These compounds have been considered as starting point for further hit-to-lead optimization, for which compound **CR** (IC_{50} = 37.25 μM) has represented an encouraging "hit compound"; the Figure 2 shows its plausible binding mode into the allosteric site of integrase catalytic core domain (CCD).

As result of this study, the carboxylic function seems to form hydrogen bonds with the IN backbone nitrogen atoms of Glu170 and His171 residues, the same interactions mediated by LEDGF/p75 hotspot residue of Asp366.[47] Additionally, a hydrogen bond with the hydroxyl group of the IN side chain of the Thr174 residue is highlighted. The remaining portion of the molecule is housed within the dimer interface cleft made up by IN chain A residues Thr174, Gln168, Ala169 and Met178 and IN chain B residues Leu102, Ala 128, Ala129 and Trp131. Thereby it is able to establish hydrophobic contacts with both the CCD subunits. The interactions between the IN CCD and compound **CR** were examined using PyMOL[48] and LIGPLUS.[49]

Considering these docking results, further efforts can be made to perform structural modifications on the different moieties of **CR** compound, in order to study the structural requirements for PPIIs and to design new coumarin derivatives. Thus, keeping unchanged both the coumarin "core"

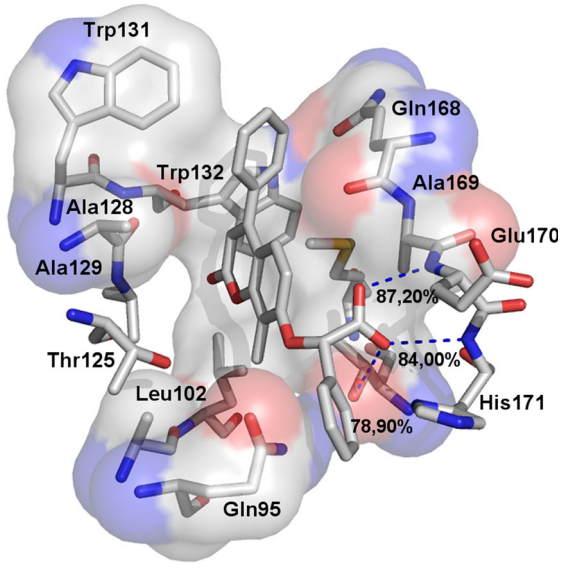

Figure 2. Binding mode of reference compound **CR** in complex with IN CCD. Key residues of the pocket are presented. Hydrogen bonds are shown by dotted lines as well as their occupancies during MD simulations as percentage. The figure was created using PyMOL software.

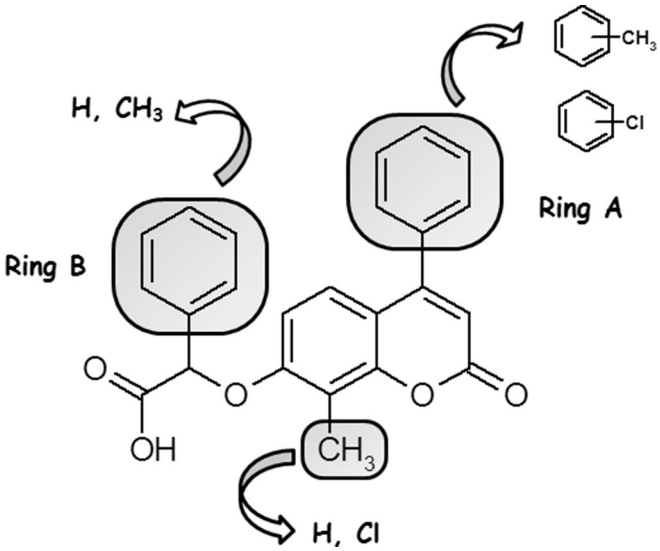

Figure 3. Design strategy for achieving new coumarin derivatives.

and carboxylic group, we decided to explore the role of the two phenyl rings (A and B) and 8-methyl group. The designed modifications are displayed in Figure 3.

Specifically, we focused on the substitutions at the phenyl ring A to explore the interaction within the hydrophobic cavity formed by Ala128, Trp131, Trp132 and Met178 residues. The structural modifications on phenyl ring A have been suggested by the pattern of substituents of other discovered LEDGF/p75 inhibitors (see Figure 1).

Then, we replaced the 8-methyl group with a chlorine atom to investigate the role of hydrophobic interaction as well as the electronic properties of the methyl substituent. We also studied the 8-unsubstituted analogs. To obtain more information about the hydrophobic area neighboring carboxyl moiety, the phenyl ring B has been removed and it has been replaced with one or two methyl groups.

3.2 Synthesis

As shown in Scheme 1, the synthesis of designed coumarin derivatives **6**, **23**–**30** has been carried out through a classic Pechmann condensation. The unsubstituted (**1**) or substituted (**2**, **3**) resorcinol reacted with malic acid or the suitable ethyl benzoylacetate to give intermediates **4** and **7**–**14**, which were alkylated by treatment with ethyl bromophenyl acetate and potassium carbonate in acetone. Finally, the obtained derivatives **5** and **15**–**22** were converted into the target compounds **6** and **23**–**30** by hydrolysis at room temperature in basic medium.

Following a similar procedure, the synthesis of compounds **35**–**37** was performed (Scheme 1). Specifically, the reaction between methyl resorcinol (**3**) and ethyl benzoylacetate furnished coumarine scaffold **31**. It was treated with the suitable ethyl bromo derivatives to give the ethyl ester intermediates **32**–**34**. Finally, the desired carboxylic acid derivatives **35**–**37** were generated by saponification with NaOH aqueous solution.

3.3 Biological Results

The synthesized coumarin derivatives were tested in AlphaScreen assay in order to evaluate their inhibitory effects on the IN-LEDGF/p75 protein interaction, and the biological results were compared with the reference compound **CR**.

As reported in Table 1, we found that all new derivatives inhibited IN-LEDGF/p75 interaction, displaying a percentage of inhibition ranging from 31% to 88%, at fixed-dose of 100 μM. On the basis of structural modifications summarized in Figure 3, we can collect the following SAR considerations. Removal of ring A (**6**) and ring B (**35**), or replacement of the latter with small alkyl groups (**36**, **37**), negatively affects the inhibition of the IN-LEDGF/p75 interaction.

Similarly substitution of 8-methyl group of the coumarin scaffold with chlorine atom was unfavorable for the PPI inhibitory effects.

On the contrary the best results were observed for derivatives **27** ($IC_{50}=60.80$ μM), **28** ($IC_{50}=60.42$ μM) and **29** ($IC_{50}=32.10$ μM) in which, keeping unchanged both the methyl group on the benzene fused ring and the unsubstituted ring B, a methyl group or a chlorine atom on the ring A have been inserted.

Table 1. Inhibition of IN-LEDGF/p75 interaction of compounds **6**, **23**–**30** and **35**–**37**

Cpd	% [a]	IC_{50}(μM) [b]	R	R′	R″	R‴
6	36	>100	CH_3	C_6H_5	—	—
23	75	>100	H	H	C_6H_5	H
24	33	>100	Cl	H	C_6H_5	H
25	47	>100	CH_3	2-Cl	C_6H_5	H
26	73	>100	CH_3	3-Cl	C_6H_5	H
27	55	60.80±2.2	CH_3	4-Cl	C_6H_5	H
28	71	60.42±2.4	CH_3	2-CH_3	C_6H_5	H
29	88	32.10±2.8	CH_3	3-CH_3	C_6H_5	H
30	78	>100	CH_3	4-CH_3	C_6H_5	H
35	29	ND	CH_3	H	H	H
36	31	ND	CH_3	H	CH_3	H
37	73	100±4.5	CH_3	H	CH_3	CH_3
CR	87	37.25	CH_3	H	C_6H_5	H

[a] % inhibition at 100 μM; [b] C_{50}: Concentration required to inhibit the HIV-1 IN-LEDGF/p75 interaction by 50%. ND: Not Determined.

3.4 Computational Studies

In order to rationalize the obtained results, the binding mode of the designed compounds was studied. The docking calculation into the LEDGF/p75-IBD binding pocket in the CCD of IN (PDB ID: 2B4J) was realized using GOLD (Genetic Optimization for Ligand Docking) software package.[50] So as to take into account the flexible side chain of residue

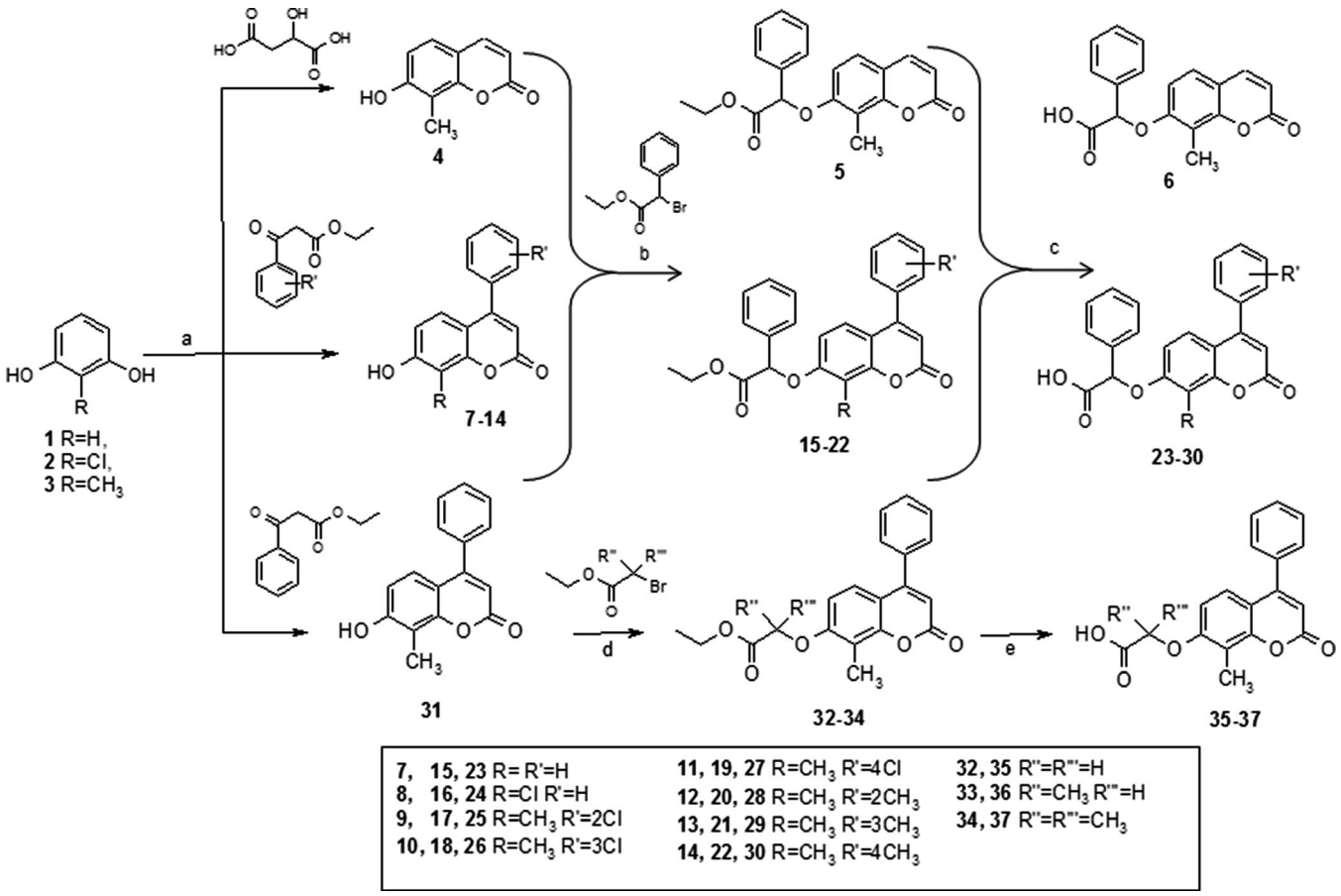

Scheme 1. Reagents and conditions: (a) H_2SO_4, rt, 3 h; (b) ethyl bromophenyl acetate, dry K_2CO_3, acetone, 110 °C, 5 h; (c) EtOH, NaOH, rt, 1,5 h. (d) suitable ethyl bromoacetate, dry K_2CO_3, acetone, 110 °C, 5 h; (e) EtOH, NaOH, rt, 1,5 h.

Gln95, two different conformations of IN CCD were used. Two clusters were taken for additional analysis.

To eliminate bad contacts, the geometry of the systems was minimized using the steepest descent algorithm followed by a conjugate gradient. The solvent effects were considered through the generalized Born implicit solvent model.

The output complex was used to estimate ligand binding free energy using the MM-GBSA[51] method ([ΔG_{bind}(complex), Table 2]) followed by additional analysis applying ultrashort Molecular Dynamics simulations using Sander module of AMBER 11.[52] The resulting system was used to estimate the binding affinity averaged over snapshots taken from the MD trajectories using the MM-GBSA method ([ΔG_{bind}(snapshots average), Table 2]). This procedure allowed us to illustrate the behavior of the complex IN-ligands.

Specifically we observed that the ranking of the predicted binding free energies are in good agreement with the experimental IC_{50} except for low active inhibitor **25**.

With the aim of highlighting stable and unstable hydrogen bonding of the starting structure, H-bond interactions with hot-spot residues were calculated by AMBER 11 considering all steps of the MD simulation and are shown in Table 3; when the occupancies were more than 20% in the investigated time period; distances between involved atoms are also indicated.

Table 2. Binding free energy estimation

compound	ΔG_{bind} (complex) kcal/mol	ΔG_{bind} (snapshots average) kcal/mol
6	−20.9	−22.6
23	−24.2	−26.7
24	−27.7	−28.7
25	−33.4	−31.9
26	−26.7	−24.1
27	−29.0	−30.2
28	−29.1	−32.1
29	−29.5	−32.9
30	−26.1	−31.2
35	−25.7	−21.9
36	−26.2	−22.7
37	−25.7	−25.2
CR	−31.8	−29.0

Table 3. Hydrogen bonds analysis from the results of MD simulation for IN in complex with compound **CR** and the designed compounds.

IN complex with	donor	acceptor	Occupancy (%) [a]	Distance (Å) [b]
	Thr174(A) OH	O3	72.4	2.935 (0.24)
	Glu170(A) NH	O3	89.4	2.863 (0.14)
6	Glu170(A) NH	O4	18.9	3.036 (0.22)
	His171(A) NH	O3	16.5	3.199 (0.20)
	His171(A) NH	O4	32.6	3.054 (0.18)
	Thr174(A) OH	O3	46.1	2.834 (0.22)
	Glu170(A) NH	O3	64.9	2.981 (0.20)
23	Glu170(A) NH	O4	46.9	2.950 (0.19)
	His171(A) NH	O3	41.4	3.075 (0.18)
	His171(A) NH	O4	10.3	3.064 (0.20)
	Thr174(A) OH	O3	40.1	2.917 (0.19)
	Glu170(A) NH	O3	58.2	2.934 (0.22)
24	Glu170(A) NH	O4	56.7	2.977 (0.20)
	His171(A) NH	O3	36.4	3.175 (0.18)
	His171(A) NH	O4	12.5	3.085 (0.21)
	Thr174(A) OH	O3	83.2	2.901 (0.23)
	Glu170(A) NH	O3	90.7	2.945 (0.18)
25	Glu170(A) NH	O4	87.3	3.038 (0.19)
	His171(A) NH	O3	70.9	3.130 (0.18)
	Thr174(A) OH	O3	7.4	2.943 (0.24)
	Glu170(A) NH	O3	87.4	2.933 (0.18)
26	Glu170(A) NH	O4	14.7	3.018 (0.23)
	His171(A) NH	O3	6.4	3.183 (0.16)
	Thr174(A) OH	O3	78.8	2.879 (0.23)
27	Glu170(A) NH	O3	86.0	2.958 (0.19)
	Glu170(A) NH	O4	84.2	3.011 (0.20)
	His171(A) NH	O3	59.3	3.064 (0.19)
	Thr174(A) OH	O3	83.7	2.885 (0.23)
28	Glu170(A) NH	O3	91.7	2.942 (0.17)
	Glu170(A) NH	O4	81.0	3.095 (0.18)
	His171(A) NH	O3	58.6	3.052 (0.17)
	Thr174(A) OH	O3	82.2	2.926 (0.25)
29	Glu170(A) NH	O3	87.0	2.976 (0.18)
	Glu170(A) NH	O4	97.7	3.021 (0.20)
	His171(A) NH	O3	95.6	3.052 (0.17)
	Thr174(A) OH	O3	75.4	2.909 (0.24)
30	Glu170(A) NH	O3	89.5	2.973 (0.20)
	Glu170(A) NH	O4	75.0	3.002 (0.19)
	His171(A) NH	O3	93.1	3.064 (0.18)
	Thr174(A) OH	O3	29.6	2.946 (0.27)
	Glu170(A) NH	O3	58.4	2.917 (0.20)
35	Glu170(A) NH	O4	46.9	2.946 (0.27)
	His171(A) NH	O3	23.0	3.182 (0.19)
	His171(A) NH	O4	10.8	3.222 (0.20)
	Thr174(A) OH	O3	54.4	2.948 (0.25)
36	Glu170(A) NH	O4	78.1	3.012 (0.22)
	Glu170(A) NH	O3	70.9	2.942 (0.19)
	His171(A) NH	O3	34.5	3.242 (0.18)
	Thr174(A) OH	O3	59.9	2.982 (0.25)
	Glu170(A) NH	O4	80.7	2.902 (0.18)
37	Glu170(A) NH	O3	52.8	3.067 (0.21)
	His171(A) NH	O3	34.5	3.182 (0.20)
	His171(A) NH	O4	13.4	3.144 (0.19)
	Thr174(A) OH	O3	88.6	2.871 (0.24)
	Glu170(A) NH	O4	97.3	2.873 (0.15)
CR	Glu170(A) NH	O3	42.7	3.123 (0.20)
	His171(A) NH	O3	47.8	3.182 (0.18)
	His171(A) NH	O4	19.4	3.087 (0.21)

[a] The listed donor and acceptor pairs satisfy the criteria for the hydrogen bond over 20.0% occupancy during the entire simulation. [b] The average distance between the hydrogen-acceptor atom and hydrogen-donor atom in the investigated time period with standard error (SE = standard deviation/N1/2) in parentheses.

3.5 Results Analysis

The insertion of substituents on the ring A (**23**–**30**) showed a significant influence on the inhibitory profile. With the aim of explaining the best activity of {[8-methyl-4-(3-methylphenyl)-2-oxo-2*H*-chromen-7-yl]oxy}phenyl)acetic acid (**29**), we analyzed its binding pose as shown in Figure 4.

To predict the impact of performed structural modifications on binding affinity, we used ultrashort molecular dynamics. As results the binding energy over snapshots average of compound **29** (Table 2) is better both than the reference compound **CR** and the other compounds displaying substitution on ring A (**25**–**28** and **30**).

Additionally, hydrogen bond analysis revealed that the carboxylate forms the same contacts with residues Glu170, His171 and Thr174 of IN, and the lipophilic group is well lodged in the hydrophobic pocket formed by residues Ala128, Trp131, Trp132 and Met178 of IN. Moreover, compound **29** showed a 97% occupancy with Glu170 and the contact between the carboxylic acid and backbone NH of the His171 was increased by 50% corresponding to the reference compound CR.

On the contrary, the removal of ring A (**6**) from the structure unfavorably affects the biological results (36% of inhibition) highlighting the importance of this ring. Figure 5 displays the binding mode of compound **6** (blue) into the IN allosteric binding site and the alignment with "reference compound" **CR** (magenta). The binding mode of **6** suggested the relevant role of the ring A for the hydrophobic contacts. Moreover, the binding energy analysis and hydrogen bond occupancies (Table 2) also confirmed that the deletion of this ring generates a molecule with a low affinity (Table 1).

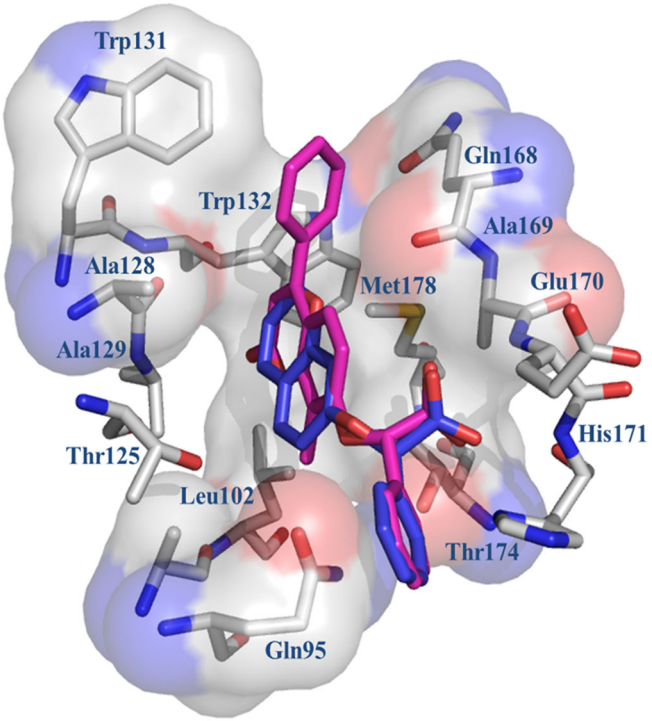

Figure 5. Binding mode of compound **6** (blue) and the reference compound **CR** (magenta) in complex with IN CCD. Key residues of the pocket are presented. The figure was created using PyMOL software.

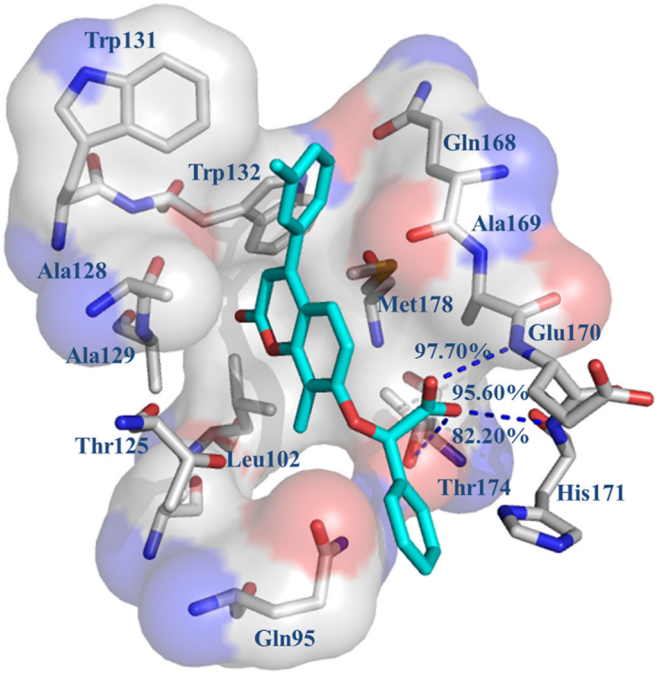

Figure 4. Binding mode of {[8-methyl-4-(3-methylphenyl)-2-oxo-2H-chromen-7-yl]oxy}(phenyl)acetic acid (**29**) in complex with IN CCD. Key residues of the pocket are presented. Hydrogen bonds are shown by dotted lines as well as their occupancies during MD simulations as percentage. The figure was created using PyMOL software.

Concerning the ring B, the removal (i.e. compound **35**) or replacement with small alkyl groups (**36**, **37**) determined detrimental effects on the binding IN-LEDGF/p75 inhibition thus highlighting the significant role of this portion for the biological profile for this class of compounds. In figure 6, the exploration of binding mode of compounds **35**–**37** is reported. There was a slightly different binding mode in comparison with to the reference compound **CR** (Figure 6) due to shift of the carboxylic acid that was revealed by the distance measurement (Table 3). This movement has affected the stability of the complex, which was illustrated also by the decrease of binding energy and the hydrogen bond occupancies, lower than **CR** compound especially for the Thr174 and the His171.

Similarly, the removal of the 8-methyl group (e.g. **23**) and its replacement by chlorine atom (**24**) was not favorable for the PPI inhibitory effects. It was observed that these modifications faintly affected the binding mode of compounds **23** and **24** in comparison with **CR** (Figure 7). These findings were highlighted by the measurement of the distances be-

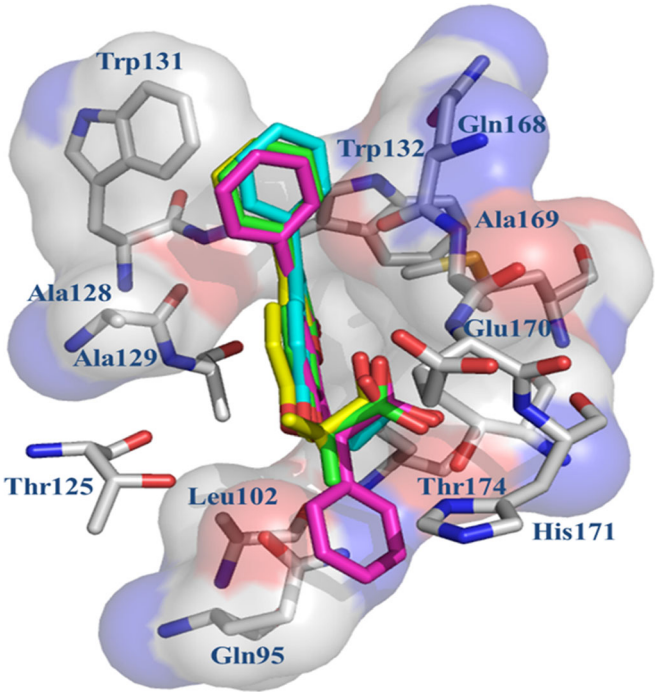

Figure 6. Binding mode of compound **35** (cyan), **36** (green), **37** (yellow) and the reference compound **CR** (magenta) in complex with IN CCD. Key residues of the pocket are presented. The figure was created using PyMOL software.

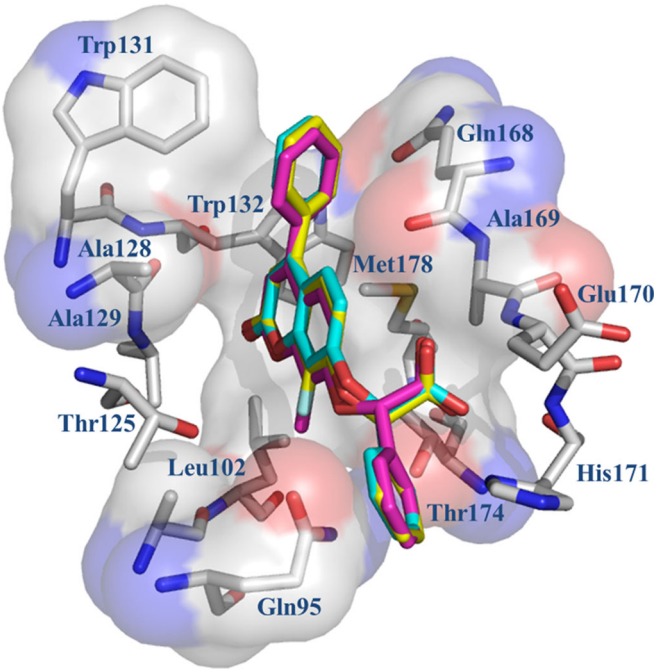

Figure 7. Binding mode of compound **23** (cyan), **24** (yellow) and the reference compound **CR** (magenta) in complex with IN CCD. Key residues of the pocket are presented. The figure was created using PyMOL software.

tween carboxylic acids in regards to the reference compound **CR**. Furthermore, the analysis of hydrogen bond occupancies (Table 3) showed a decreasing by 20 to 55% with Glu170, His171 and Thr174 for the **23** and **24** derivatives.

To obtain more information about the interaction within the IN-LEDGF interface, we compared the docking-predicted binding mode of **29** with the crystallized position of more potent inhibitors CX0516 and KF116 (Figure 8). As results, we found the overlapping of the carboxylic group for all analysed compounds. Whereas a different orientation has been found in the occupancy of the hydrophobic area lined by Ala128 and Trp131. These findings could furnish new suggestion for the design on new analogues.

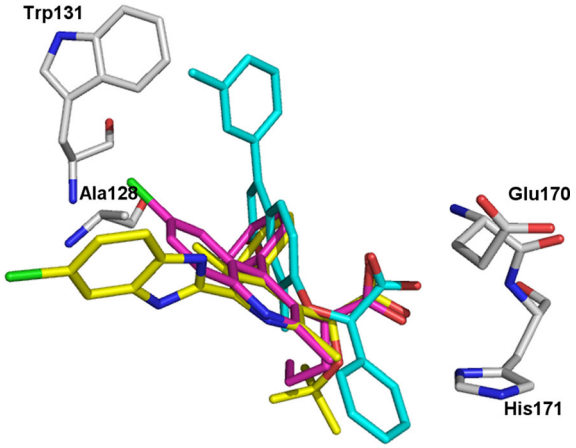

Figure 8. Docking-predicted binding mode of **29** compared to crystallized position of HIV-1 IN CCD in complex with CX0516 (magenta, pdb code: 3LPU) and KF116 (yellow, pdb code: 4O5B). The figure was created using PyMOL software.

4 Conclusions

To aim of improving inhibitory activity of our reference molecule **CR** and achieving new information about the mechanism of action, a series of modifications on the coumarin scaffold was planned and carried out. The new synthesized compounds **6**, **23**–**37** were evaluated to establish their ability to block the IN-LEDGF/p75 interaction. The best biological results were obtained for derivatives **27**–**29**, which were able to inhibit the PPI at micromolar concentration ranging from 60.42 to 32.10 μM. Specifically, for compound **29** we found that the IC_{50} value was very similar to reference compound **CR**. An extensive SAR has been discussed considering docking and molecular dynamic simulations.

Conflict of Interest

None declared.

Acknowledgements

This work was supported by University of Messina Research & Mobility 2015 Project (Project Code: RES_AND_MOB_2015_DE_LUCA).

References

[1] UNAIDS 2015. Global AIDS Response Progress Reporting **2015**.
[2] D. Zhao, K. Lu, *J. Mol. Model.* **2015**, *21*, 299.
[3] E. De Clercq, *Int. J. Antimicrob. Agents* **2009**, *33*, 307–320.
[4] Y. Mehellou, E. De Clercq, *J. Med. Chem.* **2010**, *53*, 521–538.
[5] T. Juday, S. Gupta, K. Grimm, S. Wagner, E. Kim, *HIV Clin. Trials* **2011**, *12*, 71–78.
[6] A. Ammassari, M. P. Trotta, N. Shalev, P. Marconi, A. Antinori, *Antivir. Ther.* **2012**, *17*, 785–792.
[7] P. Ryscavage, S. Kelly, J. Z. Li, P. R. Harrigan, B. Taiwo, *Antimicrob. Agents. Chemother.* **2014**, *58*, 3585–3598.
[8] S. A. Riddler, R. Haubrich, A. G. DiRienzo, L. Peeples, W. G. Powderly, K. L. Klingman, K. W. Garren, T. George, J. F. Rooney, B. Brizz, U. G. Lalloo, R. L. Murphy, S. Swindells, D. Havlir, J. W. Mellors, *N. Engl. J. Med.* **2008**, *358*, 2095–2106.
[9] S. A. Bozzette, C. F. Ake, H. K. Tam, S. W. Chang, T. A. Louis, *N. Engl. J. Med.* **2003**, *348*, 702–710.
[10] P. W. Hruz, *Curr. Opin. HIV AIDS* **2008**, *3*, 660–665.
[11] L. De Luca, S. Ferro, F. Morreale, A. Chimirri, *Mini Rev. Med. Chem.* **2011**, *11*, 714–727.
[12] L. De Luca, S. Ferro, F. Morreale, S. De Grazia, A. Chimirri, *ChemMedChem* **2011**, *6*, 1184–1191.
[13] J. Demeulemeester, P. Chaltin, A. Marchand, M. De Maeyer, Z. Debyser, F. Christ, *Expert. Opin. Ther. Pat.* **2014**, *24*, 609–632.
[14] F. Christ, Z. Debyser, *Virology* **2013**, *435*, 102–109.
[15] S. Hare, F. Di Nunzio, A. Labeja, J. Wang, A. Engelman, P. Cherepanov, *PLoS Pathog.* **2009**, *5*, e1000515.
[16] G. Maertens, P. Cherepanov, W. Pluymers, K. Busschots, E. De Clercq, Z. Debyser, Y. Engelborghs, *J. Biol. Chem.* **2003**, *278*, 33528–33539.
[17] M. Llano, M. Vanegas, O. Fregoso, D. Saenz, S. Chung, M. Peretz, E. M. Poeschla, *J. Virol.* **2004**, *78*, 9524–9537.
[18] K. Busschots, A. Voet, M. De Maeyer, J. C. Rain, S. Emiliani, R. Benarous, L. Desender, Z. Debyser, F. Christ, *J. Mol. Biol.* **2007**, *365*, 1480–1492.
[19] S. Rahman, R. Lu, N. Vandegraaff, P. Cherepanov, A. Engelman, *Virology* **2007**, *357*, 79–90.
[20] S. Emiliani, A. Mousnier, K. Busschots, M. Maroun, B. Van Maele, D. Tempe, L. Vandekerckhove, F. Moisant, L. Ben-Slama, M. Witvrouw, F. Christ, J. C. Rain, C. Dargemont, Z. Debyser, R. Benarous, *J. Biol. Chem.* **2005**, *280*, 25517–25523.
[21] M. C. Shun, J. E. Daigle, N. Vandegraaff, A. Engelman, *J. Virol.* **2007**, *81*, 166–172.
[22] H. M. Marshall, K. Ronen, C. Berry, M. Llano, H. Sutherland, D. Saenz, W. Bickmore, E. Poeschla, F. D. Bushman, *PLoS One* **2007**, *2*, e1340.
[23] A. Hombrouck, J. De Rijck, J. Hendrix, L. Vandekerckhove, A. Voet, M. De Maeyer, M. Witvrouw, Y. Engelborghs, F. Christ, R. Gijsbers, Z. Debyser, *PLoS Pathog.* **2007**, *3*, e47.
[24] F. Christ, S. Shaw, J. Demeulemeester, B. A. Desimmie, A. Marchand, S. Butler, W. Smets, P. Chaltin, M. Westby, Z. Debyser, C. Pickford, *Antimicrob. Agents Chemother.* **2012**, *56*, 4365–4374.
[25] F. Christ, A. Voet, A. Marchand, S. Nicolet, B. A. Desimmie, D. Marchand, D. Bardiot, N. J. Van der Veken, B. Van Remoortel, S. V. Strelkov, M. De Maeyer, P. Chaltin, Z. Debyser, *Nat .Chem. Biol.* **2010**, *6*, 442–448.
[26] J. J. Kessl, N. Jena, Y. Koh, H. Taskent-Sezgin, A. Slaughter, L. Feng, S. de Silva, L. Wu, S. F. Le Grice, A. Engelman, J. R. Fuchs, M. Kvaratskhelia, *J. Biol .Chem.* **2012**, *287*, 16801–16811.
[27] L. De Luca, F. Morreale, F. Christ, Z. Debyser, S. Ferro, R. Gitto, *Eur. J. Med. Chem.* **2013**, *68*, 405–411.
[28] L. De Luca, S. Ferro, F. Morreale, A. Chimirri, *Mini-Reviews in Medicinal Chemistry* **2011**, *11*, 714–727.
[29] A. Sharma, A. Slaughter, N. Jena, L. Feng, J. J. Kessl, H. J. Fadel, N. Malani, F. Male, L. Wu, E. Poeschla, F. D. Bushman, J. R. Fuchs, M. Kvaratskhelia, *PLoS Pathog.* **2014**, *10*, e1004171.
[30] D. J. Newman, G. M. Cragg, *J. Nat. Prod.* **2012**, *75*, 311–335.
[31] Y. W. Chin, M. J. Balunas, H. B. Chai, A. D. Kinghorn, *AAPS J.* **2006**, *8*, E239–253.
[32] S. Robert, C. Bertolla, B. Masereel, J. M. Dogne, L. Pochet, *J. Med. Chem.* **2008**, *51*, 3077–3080.
[33] R. Frederick, S. Robert, C. Charlier, J. de Ruyck, J. Wouters, B. Pirotte, B. Masereel, L. Pochet, *J. Med. Chem.* **2005**, *48*, 7592–7603.
[34] T. Taechowisan, C. Lu, Y. Shen, S. Lumyong, *J Cancer Res Ther* **2007**, *3*, 86–91.
[35] M. Itoigawa, C. Ito, H. T. Tan, M. Kuchide, H. Tokuda, H. Nishino, H. Furukawa, *Cancer Lett* **2001**, *169*, 15–19.
[36] V. Reutrakul, P. Leewanich, P. Tuchinda, M. Pohmakotr, T. Jaipetch, S. Sophasan, T. Santisuk, *Planta Med.* **2003**, *69*, 1048–1051.
[37] C. Spino, M. Dodier, S. Sotheeswaran, *Bioorg. Med. Chem. Lett.* **1998**, *8*, 3475–3478.
[38] H. A. Stefani, K. Gueogjan, F. Manarin, S. H. Farsky, J. Zukerman-Schpector, I. Caracelli, S. R. Pizano Rodrigues, M. N. Muscara, S. A. Teixeira, J. R. Santin, I. D. Machado, S. M. Bolonheis, R. Curi, M. A. Vinolo, *Eur. J. Med. Chem.* **2012**, *58*, 117–127.
[39] L. De Luca, M. L. Barreca, S. Ferro, F. Christ, N. Iraci, R. Gitto, A. M. Monforte, Z. Debyser, A. Chimirri, *ChemMedChem* **2009**, *4*, 1311–1316.
[40] L. De Luca, S. Ferro, R. Gitto, M. L. Barreca, S. Agnello, F. Christ, Z. Debyser, A. Chimirri, *Bioorg. Med. Chem.* **2010**, *18*, 7515–7521.
[41] L. De Luca, R. Gitto, F. Christ, S. Ferro, S. De Grazia, F. Morreale, Z. Debyser, A. Chimirri, *Antiviral. Res.* **2011**, *92*, 102–107.
[42] L. De Luca, F. Morreale, A. Chimirri, *J. Chem. Inf. Model.* **2012**, *52*, 3245–3254.
[43] S. Ferro, L. De Luca, G. Lo Surdo, F. Morreale, F. Christ, Z. Debyser, R. Gitto, A. Chimirri, *Bioorg. Med. Chem.* **2014**, *22*, 2269–2279.
[44] S. Ferro, L. De Luca, F. Morreale, F. Christ, Z. Debyser, R. Gitto, A. Chimirri, *J. Enzyme Inhib. Med. Chem.* **2014**, *29*, 237–242.
[45] S. Ferro, L. De Luca, F. E. Agharbaoui, F. Christ, Z. Debyser, R. Gitto, *Bioorg. Med. Chem.* **2015**, *23*, 3208–3214.
[46] L. Q. Al-Mawsawi, F. Christ, R. Dayam, Z. Debyser, N. Neamati, *FEBS Lett.* **2008**, *582*, 1425–1430.
[47] P. Cherepanov, A. L. Ambrosio, S. Rahman, T. Ellenberger, A. Engelman, *Proc. Natl. Acad. Sci. USA* **2005**, *102*, 17308–17313.
[48] The PyMOL Molecular Graphics System, DeLano Scientific LLC.
[49] R. A. Laskowski, M. B. Swindells, *J .Chem. Inf. Model.* **2011**, *51*, 2778–2786.
[50] G. Jones, P. Willett, R. C. Glen, A. R. Leach, R. Taylor, *J. Mol. Biol.* **1997**, *267*, 727–748.
[51] P. A. Kollman, I. Massova, C. Reyes, B. Kuhn, S. Huo, L. Chong, M. Lee, T. Lee, Y. Duan, W. Wang, O. Donini, P. Cieplak, J. Srini-

vasan, D. A. Case, T. E. Cheatham, 3rd, *Acc. Chem. Res.* **2000**, *33*, 889–897.
[52] D. A. Darden, T. A. Case, T. E. Cheatham, III, C. L. Simmerling, J. Wang, R. E. Duke, R. Luo, R. C. Walker, W. Zhang, K. M. Merz, B. Roberts, B. Wang, S. Hayik, A. Roitberg, G. Seabra, I. Kolossváry, K. F. Wong, F. Paesani, J. Vanicek, J. Liu, X. Wu, S. R. Brozell, T. Steinbrecher, H. Gohlke, Q. Cai, X. Ye, J. Wang, M.-J. Hsieh, G. Cui, D. R. Roe; D. H. Mathews, M. G. Seetin, C. Sagui, V. Babin, T. Luchko, S. Gusarov, A. Kovalenko, P. A. Kollman, Amber 11. San Francisco: University of California **2010**.
[53] R. Pauwels, J. Balzarini, M. Baba, R. Snoeck, D. Schols, P. Herdewijn, J. Desmyter, E. De Clercq, *J. Virol. Methods* **1988**, *20*, 309 – 321.
[54] Accelrys, Catalyst: http://www.accelrys.com.
[55] S. Maignan, J. P. Guilloteau, Q. Zhou-Liu, C. Clement-Mella, V. Mikol, *J. Mol. Biol.* **1998**, *282*, 359 – 368.
[56] Maestro, Schrödinger, LLC, New York, NY.
[57] Y. Duan, C. Wu, S. Chowdhury, M. C. Lee, G. Xiong, W. Zhang, R. Yang, P. Cieplak, R. Luo, T. Lee, J. Caldwell, J. Wang, P. Kollman, *J. Comput. Chem.* **2003**, *24*, 1999 – 2012.
[58] J. Wang, R. M. Wolf, J. W. Caldwell, P. A. Kollman, D. A. Case, *J. Comput. Chem.* **2004**, *25*, 1157 – 1174.

Received: December 14, 2015
Accepted: June 1, 2016
Published online: ■■ ▮▮, 0000

SPECIAL ISSUE

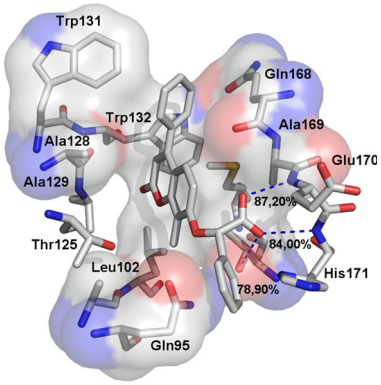

L. De Luca, F. E. Agharbaoui,* R. Gitto, M. R. Buemi, F. Christ, Z. Debyser, S. Ferro*

■■ – ■■

Rational design, synthesis and evaluation of coumarin derivatives as protein-protein interaction inhibitors